Structure of Polyelectrolyte Block Copolymer Micelles

Stephan Förster* and Nadja Hermsdorf

Universität Hamburg, Institut für Physikalische Chemie, D-20146 Hamburg, Germany

Christoph Böttcher

Freie Universität Berlin, Institut für Organische Chemie, D-14195 Berlin, Germany

Peter Lindner

Institut-Laue-Langevin, F-38042 Grenoble Cedex 9, France

Received September 4, 2001; Revised Manuscript Received February 21, 2002

ABSTRACT: The structure of charged spherical block copolymer micelles in aqueous solution was investigated with static and dynamic light scattering, small-angle neutron scattering, and cryo-electron microscopy as a function of added salt. At low added salt concentration the polyelectrolyte shell has typical features of an osmotic brush. If the added salt concentration exceeds the intrinsic ionic strength of the polyelectrolyte shell, the micellar aggregation number increases due to screening of the repulsive interaction between polyelectrolyte chains (salted brush). The relation between shell ionic strength and added salt concentration follows a simple Donnan equilibrium. The combination of methods reveals that the polyelectrolyte shell is phase-separated into a dense interior and a dilute outer domain.

1. Introduction

Polyelectrolyte block copolymers have structural features of polyelectrolytes, block copolymers, and surfactants. In dilute aqueous solutions they self-assemble into micelles consisting of a hydrophobic core and a polyelectrolyte shell. The study of their structural properties is expected to provide a basic understanding of the properties of dense polyelectrolyte layers, electrosteric stabilization mechanisms, or the physicochemical properties of the extracellular matrix.

The conformational properties of polyelectrolytes in dilute solution have been the focus of many theoretical and experimental investigations.[1,2] When densely tethered to surfaces, they represent charged polymer brushes. The properties of such polyelectrolyte brushes have been investigated theoretically by self-consistent-field theories[3−7] and scaling theories.[8,9] The variation of the brush thickness with added salt concentration or grafting density depends on whether the added salt concentration is larger or smaller than the intrinsic concentration of counterions in the brush. The two regimes are called "salted brush" and "osmotic brush", respectively. In the "osmotic brush" regime the osmotic pressure of the counterions leads to strong stretching of the polyelectrolyte chains. An increase of the added salt concentration or a decrease of grafting density has no effect on the brush height. The effect of added salt becomes considerable when the salt concentration in the bulk solution becomes comparable to or larger than the intrinsic ionic strength inside the brush. In the respective salted brush regime the brush thickness D should decrease with increasing added salt concentration according to a $D \sim c_s^{-1/3}$ scaling law. These concepts have been used to describe the properties of polyelectrolyte block copolymers micelles. The first theories on the micellization of polyelectrolyte block copolymers were published by Marko and Rabin,[10] Dan and Tirrell,[11] and Shusharina et al.[12]

Experimentally, the first systematic investigation of micelle formation of polyelectrolyte block copolymers in aqueous solutions goes back to Selb and Gallot.[13] They already noted the surprisingly low solubility of most of these polymers, when directly dissolved in water.[13,14] Since the hydrophobic domains are in most cases glassy (e.g., in the case of polystyrene), thermal energy is insufficient for spontaneous dissolution. It has since then become common practice to use organic cosolvents (DMF, dioxane, THF) for the dissolution of the polymers, followed by dialysis to obtain stable ("frozen") micelles in pure aqueous solutions.[15] Systematic studies on micellar size and structure have been published for poly(styrene-*b*-acrylic acid) (PS−PAAc),[16,17] poly(styrene-*b*-sodium acrylate) (PS−PAAcNa),[18] or quaternized poly(styrene-*b*-4-vinylpyridine) (PS−P4VPMeI).[19,20] From a comparison of the micellar core radius as measured by electron microscopy and the hydrodynamic radius as measured by dynamic light scattering, the polyelectrolyte chains in the micellar corona seemed almost fully stretched.[17] In some cases it was possible to dissolve polymers directly in water by using very short hydrophobic blocks[21] or by heating the solutions at 100 °C over a long period of time.[22,23] This enabled studies of polyelectrolyte block copolymers in aqueous solutions under equilibrium conditions.

The first sytematic investigation of equilibrium micellar properties as a function of salt concentration was performed by Guenoun et al. on poly(*tert*-butylstyrene-*b*-sodium styrenesulfonate) (PtBS−PSSNa). For $PtBS_{26}$-$PSSNa_{413}$ they observed a weak decrease of micellar size and aggregation number with increasing salt concentration.[24] The aggregation number proved independent of the salt concentration from 0.0001 to 0.01 mol/L and decreased to about half its value at high salt concentration (0.1−0.5 mol/L). The cmc of this polymer was estimated by fluorescence studies to be very low, in the range 2×10^{-7} to 2×10^{-6} g/g.[25] Using small-angle neutron scattering (SANS) of a deuterated PtBS−PSSNa(d) block copolymer, the authors could demonstrate the rodlike conformation of the polyelectrolyte chains in the micellar corona.[26]

10.1021/ma011565y CCC: $22.00
Published on Web 04/06/2002

The charged micellar corona exhibits typical features of polyelectrolyte brushes. This important analogy was investigated by Guenoun in the study of the behavior of a free-standing black film drawn from a $PtBS_{26}$-$PSSNa_{413}$ solution.[27] The thickness of these charged planar brushes as measured by X-ray reflectivity was found to decrease $D \sim c_s^{-1/3}$ when the salt concentration exceeded 0.2 mol/L. The analogy to charged brushes was further investigated by Harihanan et al., who studied the absorbed layer thickness of PtBS−PSSNa block copolymers onto latex particles.[28,29] Similarly, the layer thickness was observed to correspond to the dimensions of fully stretched corona chains at low salt concentrations. When the salt concentration exceeded a certain limit, a weak decrease of the layer thickness with increasing salt concentration was observed. Similar results have been obtained by Tauer et al.[30] when investigating electrosterically stabilized latex particles. Recent experiments on charged planar brushes are in good agreement with theoretical predictions in the osmotic and salted brush regimes.[31,32]

In the present paper we investigate the structure of spherical polyelectrolyte micelles as a function of added salt concentration. As the polyelectrolyte block copolymer we chose poly(ethylethylene-*b*-styrenesulfonic acid) (PEE−PSSH) which forms spherical micelles with a PEE core and a PSSH corona. The combination of PEE as a noncrystalline hydrophobic block having a low glass-transition temperature ($T_g = -25$ °C) with a highly charged polyelectrolyte block (PSSH) renders the block copolymers directly water-soluble even at salt concentrations as high as $c_s = 5$ mol/L. The micellar structure is characterized of by small-angle neutron scattering (SANS), static and dynamic light scattering (SLS, DLS), and cryo-transmission electron microscopy (CTEM). The experiments allow to obtain detailed structural information about the micellar core radius, the shell thickness, and density profile as well as the hydrodynamic radius of the micelle as a function of added salt.

2. Experimental Part

Block Copolymer Synthesis. Poly(ethylethylene-*b*-styrenesulfonic acid) (PEE−PSSH) was prepared by catalytic hydrogenation und subsequent sulfonation of a narrow disperse poly(styrene-*b*-butadiene) (PS−PB) as described previously.[33] The degrees of polymerization are N(PEE) = 144 and N(PSSH) = 136 with a polydispersity of $M_w/M_n = 1.04$. The degree of sulfonation was 85% as determined by the aromatic peak ratios in ^{1}H NMR.

Sample Preparation. Polymers were directly dissolved in aqueous (D_2O) salt solutions. Complete dissolution can take up to 48 h at the highest salt concentrations ($c_s > 1$ mol/L) at room temperature. At elevated temperatures ($T = 70$ °C) sample preparation takes 12 h (overnight). It was checked that the sample properties did not depend on the sample preparation procedure. The use of ultrasonic treatment was found to be unnecessary. For further analysis, the solutions were filtered through 0.8 or 0.45 μm Millipore filters. The pore size becomes an issue at high salt concentration, where large polyelectrolyte association structures are lost upon filtration when using too small pore sizes.

Static Light Scattering. Light scattering experiments were carried out at 20.0 °C. A commercial spectrometer from ALV (Langen, Germany), consisting of an ALV ISP86 goniometer and an ALV 5000 multitau correlator, was used. The measurements were performed using the $\lambda = 532$ nm line of a CW frequency-doubled, diode-pumped Nd:YAG laser (ADLAS 425c) with 300 mW output power. Toluene with an absolute scattering power of $I_{std} = 2.662 \times 10^{-5}$ cm^{-1} was used for calibration to determine the scattering volume corrected Rayleigh ratio as

$$I_R(q) = \frac{I_{sol}(q) - I_{svt}}{I_{tol}} I_{std} \left(\frac{n_{sol}}{n_{tol}}\right)^2 \quad (1)$$

where I_{sol} is the scattering intensity of the solution, I_{svt} the scattering intensity of the solvent (water), and I_{tol} the scattering intensity of toluene. The scattering vector is defined as $q = (4\pi n/\lambda) \sin(\vartheta/2)$, where n is the refractive index of the solution and ϑ the scattering angle.

The refractive index increment was determined using a scanning interferometric refractometer (NFT scan). The measured increment was $dn/dc = 0.169$ cm^3/g. From this the light scattering contrast factor factor, k (in [cm^2 mol/g^2]), can be calculated as $k_{SLS} = (4\pi^2 n^2/N_L\lambda^4)(dn/dc)^2 = 4.188 \times 10^{-7}$ cm^2 mol/g^2.

Dynamic Light Scattering. The measured normalized time-correlation function $g^{(1)}(t)$ was analyzed by use of a cumulant expansion

$$\ln g^{(1)}(q,t) = 1 - \Gamma_1(q)t + \Gamma_2(q)t^2/2 - \ldots \quad (2)$$

Γ_1 is the first cumulant which is related to the translational diffusion coefficient via $\Gamma_1 = Dq^2$. Γ_2 is the second cumulant which is related to the second moment of the distribution of relaxation times as $\Gamma_2/\Gamma_1^2 = \sigma^2$, where σ is the relative standard deviation. The diffusion coefficient can exhibit a q dependence which follows the relation

$$D(q) = D_0(1 + CR_g^2q^2 + \ldots) \quad (3)$$

where C is related to internal modes of motion of the molecules. For hard spheres $C = 0$ (no internal modes), and for flexible polymer chains $C = 0.173$. From the measured diffusion coefficient the hydrodynamic radius is obtained via the Stokes−Einstein relation

$$R_h = \frac{kT}{6\pi\eta D} \quad (4)$$

with the viscosity of water being $\eta = 0.9387$ mPa at a temperature of 296 K.

Small-Angle Neutron Scattering. The measurements were performed at the 20, 5, and 1.1 m detector position at the D11 small-angle instrument at ILL, Grenoble. The neutron wavelength was $\lambda = 0.6$ nm with a relative standard deviation of $\Delta\lambda/\lambda = 9\%$ (fwhm). Details of the instrumentation and data reduction can be found elsewhere.[34] The scattering intensity was put on absolute scale by calibration with water. The neutron contrast factor is defined as

$$k = \frac{(\Delta b)^2}{N_L} \quad (5)$$

where Δb is the contrast between polymer and solvent and N_L is Avogadro's number. The contrast Δb is given by

$$\Delta b = \left[\frac{N_L\sum_i b_{2,i}}{m_2} - \frac{v_2}{v_1}\frac{N_L\sum_i b_{1,i}}{m_1}\right] \quad (6)$$

where the b_{ij}'s are the atomic scattering cross sections of atom j in the solvent ($i = 1$) and in the monomer unit ($i = 2$) (in [cm]), m are the molecular weights of the solvent and monomer (in [g/mol]), and v are the partial specific volumes (in [cm^3/g]). To a first approximation, $v = 1/\rho$ can be used, where ρ is the bulk density (in [g/cm^3]). The neutron contrast factors k were calculated from the measured densities of PEE ($\rho = 0.8694$ g/cm^3), PSSH ($\rho = 1.550$ g/cm^3), and D_2O ($\rho = 1.106$ g/cm^3) (Paar DMA602 density meter).

Cryo-Transmission Electron Microscopy. Cryo-TEM was performed using a Philips CM12 transmission electron microscope at 100 kV. Sample grids were plunged into liquid ethane at its melting point for vitrification and imaged at $T = -175$ °C. Details can be found in ref 35.

Form Factor Analysis. To obtain a continuous set of scattering curves over a large q range, the SLS curves were shifted vertically by a constant factor equal to the ratio k_{SANS}/k_{SLS} of contrast factors (within 10%) to overlap with the SANS curves from the 20 m detector position. The slope in the overlapping q range was the same for SLS and SANS. The resulting scattering curve extends over nearly 3 orders of magnitude in scattering vector and 5 orders of magnitude in intensity. This allows a detailed analysis of the structure of polyelectrolyte block copolymer micelles.

The scattered intensity as determined by static light scattering and small-angle neutron scattering is given by

$$I(q) = kcMP_{mic}(q)\,S(q) + I_{fluc}(q) + I_{inc} \tag{7}$$

where k is the contrast factor (in [cm^2 mol/g^2]), c the polymer concentration (in [g/cm^3]), M the molecular weight (in [g/mol]), $P_{mic}(q)$ the form factor of the micelle, and $S(q)$ the structure factor. $I_{fluc}(q)$ is related to fluctuations within the micellar corona, and I_{inc} is due to the incoherent scattering of the polymer.

The form factor of the block copolymer micelles consists of contributions from the micellar core, $F_{core}(q)$, the micellar shell, $F_{shell}(q)$, and interference terms between core and shell, $F_{cs}(q)$, i.e.

$$P_{mic}(q) = (F_{core}(q) + F_{shell}(q))^2 \tag{8}$$

(see Appendix). This expression simplifies considerably, if the scattering experiments are preformed under conditions where only the micellar core or shell contribute to the scattered intensity. Then the form factor is simply $P_{mic}(q) = F_{core}^2(q)$ or $P_{mic}(q) = F_{shell}^2(q)$, respectively. In SANS experiments this can be achieved by using an appropriate mixture of deuterated and nondeuterated solvent to match either the scattering contrast of the shell or the core. If both core and shell contribute to the scattered intensity, as in the present case, then the more complicated expression in eq 8 including the interference term has to be used. However, the scattering curve then contains important information about the internal structure of the micelles. In the present paper such an analysis is performed. The form factor $P_{mic}(q)$ is given in the Appendix.

At large scattering vectors fluctuations within the micellar corona dominate the scattering intensity. Since polyelectrolyte are locally strongly stretched, the fluctuations may be described by the form factor of an infinitely thin cylinder[36] which is given by

$$I_{fluc}(q) = I_{fluc}^0\left\{\frac{2}{q\xi}\mathrm{Si}(q) - \left(\frac{\sin(q\xi/2)}{q\xi/2}\right)^2\right\} \tag{9}$$

where $\mathrm{Si}(z)$ is the sine integral, ξ is the correlation length of the fluctuations, and I_{fluc}^0 is the prefactor.

Charged micelles exhibit repulsive interaction at low salt concentrations that are noticeable as a minimum in the scattering curve at low q. For weak interactions as in the present case, these can be described by a Percus−Yevick structure factor $S(q)$.[37] At high salt concentrations there are weak attractive interactions that give rise to a weak upturn of the scattering intensity at low q. This can be described by the structure factor of fractal aggregates[43] and is described in a previous publication.[33]

As an example the analysis of a typical SLS/SANS curve as measured for $c_s = 0.01$ mol/L is shown in Figure 1. The scattering of the solvent has already been subtracted. I_{inc} is generally very low and of the order of 10^{-3} cm^{-1}. The contribution from I_{fluc} is noticeable only at large q, where the scattering of the micelle has decayed to less than 10^{-2} cm^{-1}. It exhibits a q^{-1} asymptote due to a locally stretched conformation of the polyelectrolyte chains. At intermediate q the scattering of the micellar core, $F_{core}(q)$, leads to damped oscillations with a Porod q^{-4} envelope. At lower q, the scattering is mainly due to the micellar shell. The shell contribution to the form factor of the micelle is described in more detail in the Appendix (see Figure 11).

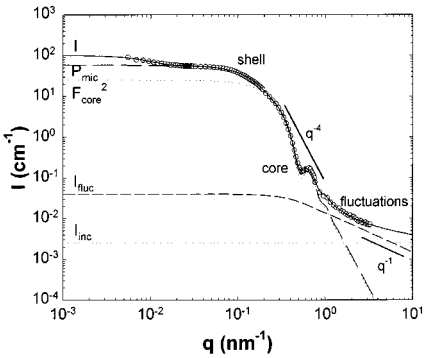

Figure 1. Contributions to the scattered intensity for block copolymer micelles.

3. Results and Discussion

Polyelectrolyte Effects. At low salt concentration, electrostatic interactions can influence the scattering behavior considerably. These interactions lead to so-called "polyelectrolyte effects" that include positional correlations, low-q upturns in the scattering curves, and the observation of a slow-mode in dynamic light scattering.[38] These phenomena occur at a ratio of polyelectrolyte (monomer) to salt concentration of $\lambda^* = c_p/c_s > 1$ for linear flexible polyelectrolyte chains.[39] They complicate the determination of size and shape of dissolved particles. This implies that investigations of single particle properties at low salt concentrions of 0.01 or 0.001 mol/L require to study polymer concentrations below 2 or 0.2 g/L, respectively. Advantageously, for dense polyelectrolyte structures like stars, spheres, or brushes, charge renormalization shifts the ratio λ^* to larger values $\lambda^* >> 1$, which allows to work at larger polymer concentrations. In our case the sample with the lowest amount of added salt ($c_s = 0.001$ mol/L at $c_p = 6$ g/L) has the largest value of $\lambda^* = 25$. We could observe neither a low-q upturn nor a slow-mode in the scattering curves, indicating that the added salt concentration is sufficiently high to screen intermicellar electrostatic interactions.

Micellar Structure. The structure of block copolymer micelles may be described in terms of the model of starlike polymer as proposed by Daoud and Cotton. Starlike polymers consist of a homogeneous, dense polymer core surrounded by a polymer layer. As a consequence of the spherical geometry, the density profile $\rho(r)$ in the polymer layer decreases as[40]

$$\rho(r) \sim Z^{\alpha/2} r^{-\alpha}, \quad \alpha = \frac{1-3\nu}{2} \tag{10}$$

Z is the number of arms in a starlike polymer or the aggregation number in the case of block copolymer micelles. ν is the Flory exponent, which has characteristic values as given in Table 1.

The corresponding density profile is schematically shown in Figure 2. Micelles consist of a well-defined micellar core with a radius R_c and a micellar shell or corona extending to the outer micellar radius R_m. The diameter of the corona is given by $D = R_m - R_c$. Within

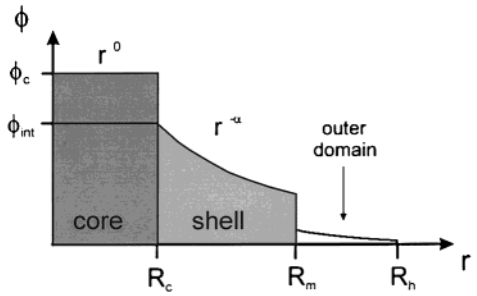

Figure 2. Schematic density profile of a block copolymer micelle. There seems to exists a very dilute outer shell domain in the case of polyelectrolyte shells as outlined in section 4.

Table 1. Flory Exponent ν and Exponent α of the Radial Density Profile for Different Thermodynamic States of the Polymer Chains

ν	α	remarks
$^1/_3$	0	collapsed polymer, core domain
$^1/_2$	1	polymer in Θ-solvent, semidilute solution
$^3/_5$	$^4/_3$	polymer in good solvent
1	2	polymer in stretched conformation, e.g., polyelectrolyte

the framework of the Daoud−Cotton model the polymer volume fraction profile $\phi(r)$is given by

$$\phi(r) = \begin{cases} \phi_c, & \text{for } 0 \le r < R_c \text{ (core)} \\ \phi_{int}\left(\frac{r}{R_c}\right)^{-\alpha}, & \text{for } R_c \le r < R_m \text{ (shell)} \\ 0, & \text{for } R_m \le r \end{cases} \quad (11)$$

with the volume fraction ϕ_c of the core and the interfacial volume fraction ϕ_{int}. Such a density profile has been shown to adequately describe the structure of strongly segregated PS−P4VP block copolymer micelles.[41] For a polymeric corona one theoretically expects values of the exponent in the range $1 \le \alpha \le {}^4/_3$ depending on the solvent quality (see Table 1). Experimentally determined values for the exponent are $1.03 \le \alpha \le 1.35$.[41,42] The form factor $P_{mic}(q)$ corresponding to this density profile can be obtained in closed analytical form and is given in the Appendix. The radius of gyration of a micelle with a structure as in Figure 2 is given by

$$R_g^2 = \frac{\frac{1}{5} + \frac{\phi_{int}}{5+\alpha}(p_1^{-(5+\alpha)} - 1)}{\frac{1}{3} + \frac{\phi_{int}}{3+\alpha}(p_1^{-(3+\alpha)} - 1)} p_1^2 R_m^2 \quad (12)$$

where $p_1 = R_c/R_m$.

Static Light Scattering (SLS) and Small-Angle Neutron Scattering (SANS). The scattering curves of the micelles at $c_p = 5$ g/L for added salt concentrations increasing from $c_s = 0.001$ to 3 mol/L are shown in Figure 3. Scattering curves at a given salt concentration have been subsequently offset by a factor of 3 to visualize them more clearly. Except at the highest salt concentrations, the scattering intensity at low q ($5 \times 10^{-3} \le q \le 10^{-1}$ nm^{-1}) is nearly q-independent. At low salt concentrations ($c_s \le 0.003$ mol/L) there is a slight depression of the scattered intensity at around $q \approx 0.03$ nm^{-1} due to intermicellar correlations arising from repulsive electrostatic interactions. At high salt concentrations ($c_s \ge 1$ mol/L) there is a significant low-q upturn of the scattered intensity due to clustering of the micelles. There is a weak decrease of $I(q)$ at

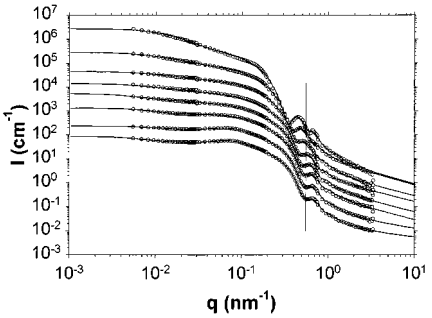

Figure 3. SLS/SANS scattering curves at a polymer concentration of $c_p = 5$g/L for salt concentrations increasing from $c_s = 0.001$ mol/L (bottom curve) over 0.003, 0.01, 0.03, 0.1, 0.3, 1 to 3 mol/L (top curve). The curves are mutually offset by a factor of 3 for better visualization; the bottom curve corresponds to an offset of 1. Solid lines are fits to eq 7. The vertical line indicates the shift of the oscillation.

intermediate q ($0.08 \le q \le 0.2$ nm^{-1}) arising from the scattering of the micelllar corona. Above $q = 0.2$ nm^{-1} the scattered intensity decays strongly, showing damped oscillations with a Porod q^{-4} envelope due to the scattering of the micellar core. At large q there is a slow q^{-1} decay arising from fluctuations within the micellar corona. The observed shift of the minimum at around $q \approx 0.5$ nm^{-1} indicates an increase of the micellar core diameter with increasing salt concentration.

A quantitative analysis is performed by fitting the measured scattering curves to a sum of the three contributions arising from the scattering of the micelles, $P_{mic}(q)$, fluctuations, $I_{fluc}(q)$, and incoherent background, I_{inc}, of the sample according to eq 7. The analytical expression for the micellar form factor $P_{mic}(q)$ is given in the Appendix. The slight depression of the scattered intensity at low salt concentrations can be described by a Percus−Yevick structure factor $S(q)$, the low-q upturn at large salt concentrations by a structure factor derived for fractal aggregates.[43] A detailed description of the aggregate structures is the topic of a separate paper.[33] Measured scattering curves were fitted by a nonlinear least-squares method using the Levenberg−Marquardt algorithm. Fits to eq 7 are indicated by the solid lines in Figure 3.

The analysis yields the micellar core radius R_c, the overall micellar radius R_m, their relative standard deviation σ_R, the relative scattering length density at the core/corona interface ρ_{int}, and the scaling exponent α. Their values for different salt concentrations are given in Table 2. The relative error of all fit parameters as determined from the covariance matrix is 1−5% except for α, where the error is 10%. The relative standard deviations of the radii σ_R are all in the range $0.10 \le \sigma_R \le 0.13$. From the radii R_c and R_m, the dimension of the corona $D = R_m - R_c$ can be calculated. Also collected in Table 2 are the radius of gyration R_g as calculated from eq 12.

From the relative scattering length density ρ_{int} the volume fraction ϕ_{int} (see Figure 2) can be calculated as

$$\phi_{int} = \frac{k_A}{k_B} \frac{\rho_A \phi_c}{\rho_B \rho_{int}} \quad (13)$$

where the $k_{A,B}$ are the contrast densities between A- and B-block and the solvent and $\rho_{A,B}$ are the (partial) specific densities of the A- and B-block (A = PEE, B = PSSH). The volume fraction ϕ_c of the micellar core is to a good

Table 2. Added Salt Concentration c_s, Core Radius R_c, Micellar Radius R_m, Exponent α, Interfacial Contrast Density ρ_{Int} As Determined by SLS/SANS, Shell Thickness $D = R_m - R_c$, Hydrodynamic Radius R_h Determined by DLS, Radius of Gyration R_g Calculated from Eq 12, Largest Possible Micellar Dimension R_{max} Calculated from Eq 14, and Ratio R_g/R_h

c_s (mol/L)	R_c (nm)	R_m (nm)	α	ρ_{int}	D (nm)	R_h (nm)	R_g (nm)	R_{max} (nm)	R_g/R_h
0.001	9.2	25.3	0.40	0.018	16.1	38.5	16.9	43.2	0.43
0.003	9.3	25.2	0.40	0.017	15.9	38.1	16.6	43.3	0.44
0.01	9.4	25.7	0.44	0.018	16.3	38.5	17.1	43.4	0.44
0.03	9.7	24.6	0.53	0.020	14.9	37.8	16.3	43.7	0.39
0.1	10.2	25.2	0.51	0.020	15.0	37.4	16.4	44.2	0.43
0.3	11.3	23.7	0.72	0.026	12.4	40.2	15.0	45.3	0.39
1.0	12.5	23.2	0.64	0.037	10.7	41.0	14.3	46.5	0.38
3.0	13.7	23.4	0.45	0.080	9.7		15.7	47.7	

approximation $\phi_c = 1$, since the hydrophobic core does not swell with water

Dynamic Light Scattering (DLS). The reduced first cumulants Γ_1/q^2 as a function of q^2 are shown in Figure 4 for various salt concentrations. On the basis of eq 3, one expects a linear dependence which, however, at low q is surprinsingly steep. The slope at low q corresponds to C values of the order 10. At high q the values of the reduced first cumulant become only sligthly depdendent on q. The slopes at high q correspond to C values between $0.01 < C < 0.05$, which are typical for block copolymer micelles.[44] The strong drop of the first cumulant is related to the presence of micellar multiplets and corresponds to the low-q upturn observed in the SLS/SANS curves. To determine the hydrodynamic radius R_h of the micelles, we use the diffusion coefficient determined from the high-q regime, i.e., $q > 0.01$ nm^{-1}, which as seen in Figure 3 corresponds to contributions that are only due to the micelles. This separation is possible up to salt concentrations > 1 mol/L. The values of the hydrodynamic radius for various salt concentrations are summarized in Table 2. Also included is the ratio R_g/R_h, which is quite sensitive to the density profile of a polymeric molecule. For spherical particles its value is independent of the molecular size and gives qualitative information about the micellar structure. Hard spheres have a value of $R_g/R_h = \sqrt{3/5} \approx 0.775$. Lower values down to $R_g/R_h = 0.58$ have been reported for small spherical microgels. The ratio determined for the micelles in the present study are given in Table 2.

Cryo-Electron Microscopy (Cryo-TEM). Using cryo-transmission electron microscopy (cryo-TEM), one obtains direct images of the polyelectrolyte micelles in their solvated state. For cryo-TEM aqueous micellar solutions are vitrified by injecting sample grids into liquid ethane at its melting point.

Figure 5 shows cryo-electron micrographs of micellar solutions ($c_p = 5$ g/L; $c_s = 0.003$ (a) and 3 mol/L (b)) which had been investigated also by SLS/SANS. Contrast arises from the electron density difference between micellar core, corona, and the surrounding salt solution. In Figure 5a ($c_s = 0.003$ mol) the micellar cores appear as gray spherical domains. The radius of the micellar core is $R_c = 9.1$ nm with $\sigma_R = 0.12$, in good agreement with results from SANS (Table 2). Addition of salt increases the electron density in the surrounding solution which leads to contrast inversion. At a salt concentration of $c_s = 3$ mol/L (Figure 5b) the micellar cores appear as bright spherical domains surrounded by the dark interior micellar corona which contains a high concentration of ionic species ($-SO_3^+$, Na^+, Cl^-). The contrast directly corresponds to the spatial distribution of these ions. The measured radii are $R_c = 13.4$ nm and $R_m = 26.3$ nm with $\sigma_R = 0.08$, in good agreement with the results from neutron scattering experiments (Table 2). The images indicate a sharp, nearly discontinuous drop of the density at R_m, which gives to scattering from the corresponding interface.

The radii R_c, R_m, R_h, and R_{max} as a function of salt concentration are shown in Figure 6. Their values are practically constant up to a salt concentration of $c_s^* \approx 0.1$ mol/L. Above c_s^* the core radius increases while the micellar radius R_m slightly decreases. Over the range

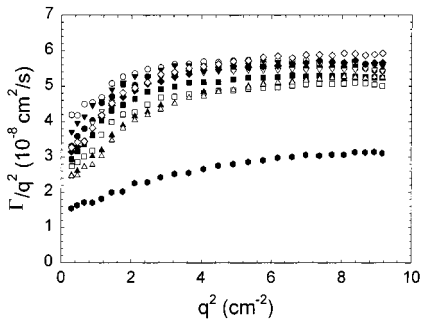

Figure 4. First cumulants Γ/q^2 as a function of q^2 for various salt concentrations: (●) 0.001, (○) 0.003, (▼) 0.006, (▽) 0.01, (■) 0.03, (□) 0.06, (◆) 0.1, (◇) 0.3, (▲) 0.6, (△) 1, and (⬡) 3 mol/L.

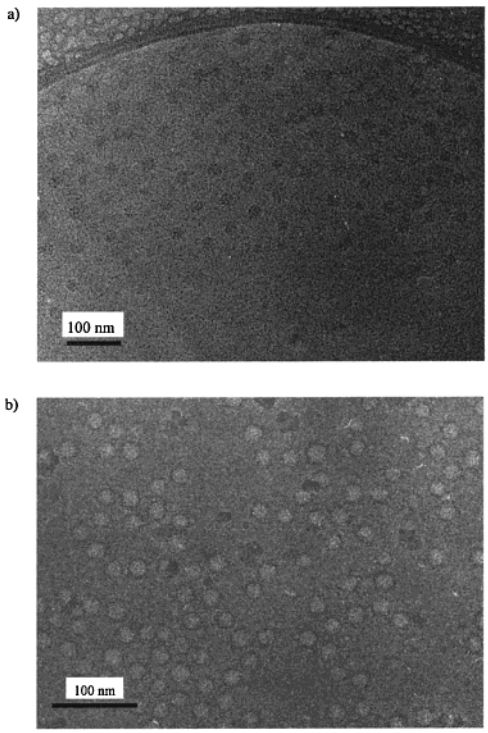

Figure 5. Cryo-electron micrographs of micellar solutions at 0.003 **(**a**)** and 3 mol/L **(**b**)** salt concentration. At high salt concentration the dense interior corona domain surrounding the micellar core is clearly visible. The scale bars are 100 nm.

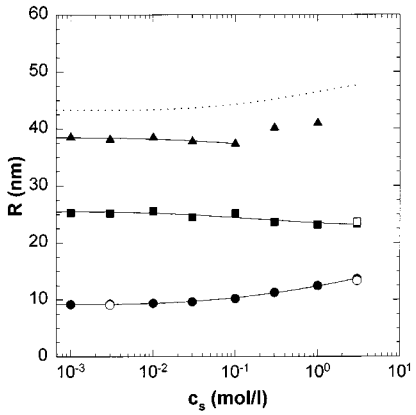

Figure 6. Measured core radius R_c (●), micellar radius R_m (■), and hydrodynamic radius R_h (▲) as a function of added salt concentration. Open symbols (O, □) were determined by cryo-electron microscopy. The dotted line corresponds to the outer micellar radius assuming fully stretched corona chains.

of salt concentrations, the hydrodynamic radius R_h is approximately constant but significantly larger than the micellar radii R_m. R_h nearly approaches the largest possible radius given by

$$R_{max} = R_c + L_{PSSH} \tag{14}$$

(dotted line in Figure 6) and corresponds to polyelectrolyte chains that are stretched to about 80% of their contour length. For a fully stretched PSSH chain the contour length is is $L = N_{PSSH} l_0 = 34.0$ nm assuming a monomer contour length of $l_0 = 0.25$ nm. Such high stretching ratios as determined by DLS were also reported by Hariharan et al.[28] for dense PSSNa brushes absorbed on polystyrene latices. At low salt concentrations of $c_s = 10^{-4}$ mol/L, they reported a layer thickness of 195 nm at a chain contour length of 201 nm.

Strong chain stretching is consistent with Pincus' prediction for the "osmotic brush" regime.[8] Also, the characteristic q^{-1} scattering at high q indicates the corona chains to be strongly stretched. This has been previously reported by Guenoun et al.[26] At concentrations above c_s* the micellar structure becomes dependent on the added salt concentration which is a characteristic of the "salted brush" regime.

Salt Dependence of Aggregation Numbers. From the measured core radius we can calculate the micellar aggregation number Z and the average distance (grafting distance) of chains at the core/corona interface, b

$$Z = \frac{4\pi R_c^{\,3}}{3 N_{PEE} v_{PEE}} \tag{15}$$

$$b^2 = \frac{4\pi R_c^{\,2}}{Z} \tag{16}$$

assuming the core to consist of a homogeneoues melt of PEE. The monomer volume is given by $v_{PEE} = m_{PEE}/(\rho_{PEE} N_L) = 0.107$ nm^3. Values for Z and b are given in Table 3.

The aggregation numbers as a function af added salt concentration are shown in Figure 7. Whereas in the *osmotic brush* regime at low added salt concentration the aggregation numbers and grafting distances are constant, at concentrations above c_s* ≈ 0.1 mol/L (*salted brush*) we observe an increase from $Z \approx 200$ to $Z \approx 700$ at large added salt concentrations. Because of screening

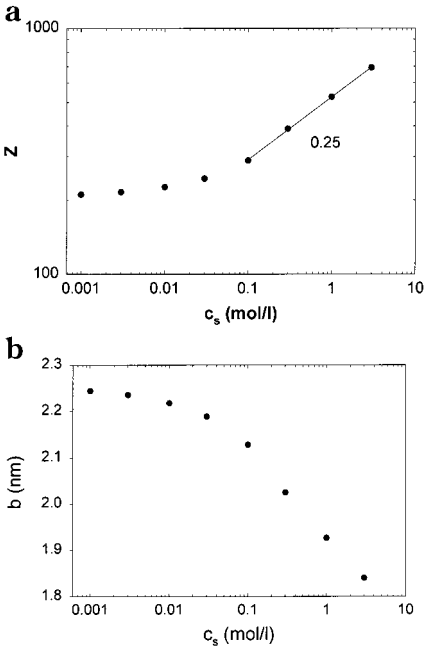

Figure 7. (a) Micellar aggregation numbers Z and (b) and grafting distances b as a function of added salt concentration.

of the repulsive interaction between corona chains, the interfacial area per chain is decreasing with increasing salt concentration accordingly. We do not observe a decrease of aggregation numbers with increasing salt concentration as reported by Guenoun et al.[24]

Salt Dependence of the Shell Dimension. According to scaling theories in the *salted brush* regime, also the layer thickness should be dependent on added salt concentrations. For spherical brushes the thickness D depends on the aggregation number Z as

$$D \sim \left(\frac{Z v_e}{l_k}\right)^{(1-\nu)/2} \tag{17}$$

where l_k is the statistical segment length of the polyelectrolyte chain and v_e the excluded volume. The aggregation number enters this equation as a consequence of the influence of the interfacial area per chain, i.e., $Z \sim a^{-3}$. For the excluded volume of polyelectrolyte chains a common approximation is to set $v_e \sim l_k \kappa^{-2}$ where $\kappa^{-1} \sim c_s^{-1/2}$ is the Debye length. This proved to give good agreement between theory and experiments on polyelectrolyte conformation as a function of added salt. For good solvents where $\nu = {}^3/_5$ one expects a scaling relation $D \sim Z^{1/5} c_s^{-1/5}$.

The corona dimension is calculated as $D = R_m - R_c$. Values of D are in the range $9.7 \le D \le 16.2$ nm. These values can be compared to the corona dimensions of planar brushes formed by the same block copolymer at the air/water interface.[32] In salt-free solutions the brush dimension is $D_{planar} = 14.1$ nm, decreasing to 6.9 nm at high salt concentrations. At high c_s the values of D_{planar} are quite small, because in the Langmuir trough the grafting density b was varied in a range between 2.2 and 4.5 nm, whereas the micelles or spherical brushes have values between 1.8 and 2.2 nm (see Table 3); i.e., the chains are much more compressed.

A plot of D vs c_s is shown in Figure 8. We observe no obvious straight linear behavior in the double-logarithmic presentation at large salt concentrations. However, the straight line drawn for comparison has a slope of

Table 3. Added Salt Concentration c_s, Aggregation Number Z (Eq 15), Grafting Distance b (Eq 16), Contrast Factors k_{PEE} and k_{PSSH}, Interfacial Volume Fraction ϕ_{int} from Eq 13, Average Shell Volume Fraction $\bar{\phi}$ from Eq 18, Shell Ionic Strength $\bar{c}_{s,int}$ from Eq 19, PSSH Block Volmes v', v'' (Shell) from Eqs 21, 22, and Volume Fraction in Outer Shell Domain ϕ_{out} (Eq 23)

c_s (mol/L)	Z	b (nm)	k_{PEE} (cm^2 mol/g^2)	k_{PSSH} (cm^2 mol/g^2)	ϕ_{int}	$\bar{\phi}$	$\bar{c}_{s,int}$ (mol/L)	v' (10^4 nm^3)	v'' (10^4 nm^3)	ϕ_{out}
0.001	218	2.21	0.009 80	0.001 20	0.084	0.063	0.57	4.1	5.3	0.007
0.003	223	2.20	0.009 80	0.001 20	0.079	0.059	0.53	3.8	5.4	0.011
0.01	234	2.18	0.009 80	0.001 20	0.083	0.060	0.54	4.1	5.7	0.010
0.03	254	2.15	0.009 80	0.001 20	0.091	0.064	0.58	3.7	6.2	0.010
0.1	300	2.09	0.009 73	0.001 18	0.092	0.067	0.60	4.2	7.3	0.019
0.3	405	1.99	0.009 62	0.001 16	0.120	0.084	0.76	4.2	9.8	0.032
1.0	545	1.90	0.009 22	0.001 09	0.168	0.130	1.17	5.7	13.2	0.043
3.0	718	1.81	0.008 27	0.000 91	0.366	0.315	2.84	13.5	17.4	

-0.13, which is in agreement with results of Guenoun et al., who reported a $D_h \sim c_s^{-0.14}$ dependence for PtBS$_{26}$-PSSNa$_{404}$ and a $D_h \sim c_s^{-0.11}$ dependence for PtBS$_{27}$-PSSNa$_{757}$ with added salt concentration.[24] Adsorbed layers of PtBS$_{27}$PSSNa$_{757}$ on polystyrene latices exhibited a $D_h \sim c_s^{-0.17}$ dependence.[29] The exponent seemed to decrease from -0.11 to -0.17 with increasing hydrophobic core radius. However, since the surface density varies in those studies and salt concentrations, a quantitative comparison is difficult.

Donnan Equilibrium. It is expected that the addition of salt affects micellar properties if the added salt concentration c_s becomes comparable to the intrinsic ionic strength within the micellar corona, $c_{s,0}$. As the chain segment concentration decreases in the radial direction, we may consider the average ionic strength of the corona and its relation to the added salt concentration. The average volume fraction of polyelectrolyte chains in the micellar the corona is given by

$$\bar{\phi}_{in} = \frac{\int_{R_c}^{R_m} \phi_{int}\left(\frac{r}{R_c}\right)^{-\alpha} 4\pi r^2 \, dr}{\int_{R_c}^{R_m} 4\pi r^2 \, dr} = \frac{3}{3-\alpha}\phi_{int}\frac{R_c^{\alpha}(R_m^{3-\alpha} - R_c^{3-\alpha})}{R_m^3 - R_c^3} \quad (18)$$

The values are collected in Table 3. From the average volume fraction we can calculate the average molar concentration of chain segments and counterions as

$$\bar{c}_{s,int} = \rho_{PSSH}\bar{\phi}_{in}/m_{PSSH} \quad (19)$$

where m_{PSSH} is the monomer molecular weight of the PSSH block. Calculated values of $\bar{c}_{s,int}$ are summarized in Table 3 and plotted as a function of added salt concentration in Figure 9.

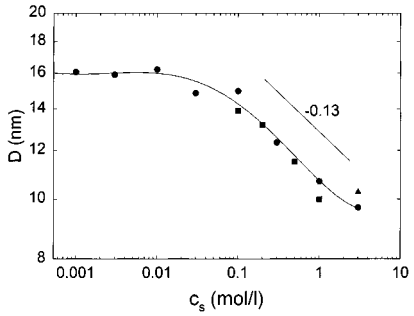

Figure 8. Salt dependence of the micellar corona thickness D (●). ■ are data taken from measurements of planar brushes of the same block copolymer (ref 32).

At low ionic strength the local ion concentration is essentially constant until it increases at larger added salt concentration. The c_s dependence follows a trend that is characteristic for the Donnan equilibrium. As derived by Hariharan et al.,[29] there should be a simple relation

$$\bar{c}_{s,int} = c_s\left[1 + \frac{c_{s,0}^2}{c_s^2}\right]^{1/2} \quad (20)$$

between $\bar{c}_{s,int}$ and c_s which allows to determine $c_{s,0}$, the intrinsic concentration of ionic species in the polyelectrolyte brush. From a fit of eq 20 to the data in Figure 9 $c_{s,0}$ can be determined to be $c_{s,0} = 0.53$ mol/L. Experimentally, changes in micellar structure are observed above an added salt concentration of $c_s^* = 0.1$ mol/L. This value is lower than the value of $c_{s,0}$ and indicates counterion condensation which reduces the ionic strength to a value of $l_0 c_{s,0}/l_B \approx 0.18$ mol/L, where $l_B = e^2/(4\pi\epsilon\epsilon_0 kT) \approx 0.72$ nm is the Bijerrum length and $l_0 = 0.25$ nm is the contour distance between successive charges on the chain. The Debye length in the corona, calculated from the interior salt concentration as $\kappa^2 = 8\pi N_L l_B c_{s,0}$, is $\kappa^{-1} \approx 0.4$ nm, which is much smaller than the grafting distance b or the smallest blob size of the spherical brush and indicates that the local electroneutrality condition which requires $\kappa^{-1} \ll b$ is well fulfilled.

It was already noted in previous studies that added salt affects the micellar structure only above a certain value of the salt concentration c_s^*. In studies of PtBS−PSSNa block copolymers a dependence of the brush dimension on the added salt concentration appeared above $c_s = 0.01$ mol/L. The thickness of a free-standing black films drawn from a diblock polyelectrolyte solution exhibited a steady drop above ionic strengths of 0.2 mol/L[27] and was found to follow a scaling relationship $L \sim c_s^{-0.31}$, in close agreement with the value predicted by Pincus.

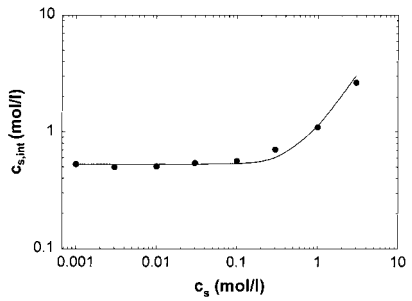

Figure 9. Internal salt concentration $\bar{c}_{s,int}$ as a function of added salt. The solid line is a fit to eq 20 according to a Donnan equilibrium.

Corona Phase Separation. At several instances we have pointed out that the polyelectrolyte corona has some unusual properties:

(i) The measured hydrodynamic radius R_h is significantly larger than the micellar radius R_m. In the case of uncharged block copolymer micelles the hydrodynamic radius is usually smaller than the micellar radius. At low added salt concentrations large hydrodynamic radii may be attributed to strong intermicellar interactions wich lead to larger effective radii. However, the observed effect is also present at large added salt concentration where such interactions are screened.

(ii) We observe very low values of the characteristic ratio $0.38 < R_g/R_h < 0.44$. Ratios measured for uncharged block copolymer micelles are usually in the range 0.7−1.4, which is typcial for starlike polymeric structures.[44] Values as low as 0.57 have been only reported for microgels with a dilute outer sphere of polymer chain segments.[45]

These effects seem to be related to a peculiar property of the polyelectrolyte shell. It can be inferred from a consideration of the volume fraction of the polyelectrolyte block (B-block) in the corona domain. In terms of the density profile given in eq 11, the total volume taken up by the polymer blocks in the core or corona ist given by

$$V = \begin{cases} \frac{4\pi}{3}R_c^3 \equiv v'_{core}, & \text{for } 0 \le r < R_c \text{ (core)} \\ \frac{4\pi}{3}\bar{\phi}(R_m^3 - R_c^3) \equiv v'_{shell}, & \text{for } R_c \le r < R_m \text{ (shell)} \\ 0, & \text{for } R_m \le r \end{cases} \quad (21)$$

Since the blocks are covalently linked, we expect

$$v'_{core} = v''_{core} \equiv ZN_A v_A$$
$$v'_{shell} = v''_{shell} \equiv ZN_B v_B \quad (22)$$

The volumes v' are calculated from SANS measurements of R_c, R_m, and ρ_{int}, whereas v'' are derived from properties of the block copolymer chains together with the aggregation number Z. $v_B = m_{PSSH}/(\rho_{PSSH}N_L) \approx 0.197$ nm^3 is the volume of a PSSH monomer unit. Assuming $v'_{core} = v''_{core}$ to be valid to calculate Z, we observe that $v'_{shell} < v''_{shell}$. The difference is between 50 and 80% of the value expected from v''_{shell}. This is quite remarkable and beyond the experimental error and means that the corona domain does *not* contain all the polyelectrolyte chain segments. The polyelectrolyte chains extend beyond R_m into an outer corona domain, possibly up to the hydrodynamic radius R_h; i.e., the micellar shell consists of a dense interior part $R_c \le r < R_m$ and a dilute outer part $R_m \le r < R_h$. This naturally explains the difference between the two radii R_m and R_h and the unusual low values of R_g/R_h.

From the missing volume $v_{out} = v''_{shell} - v'_{shell}$, we can calculate the volume fraction $\bar{\phi}_{out}$ of the outer corona domain as

$$\bar{\phi}_{out} = \frac{3v_{out}}{4\pi(R_h^3 - R_m^3)} \quad (23)$$

This then allows to construct the density profile of spherical polyelectrolyte micelles as a function of salt in a refined version, which takes into account the outer corona domain. This is shown in Figure 10.

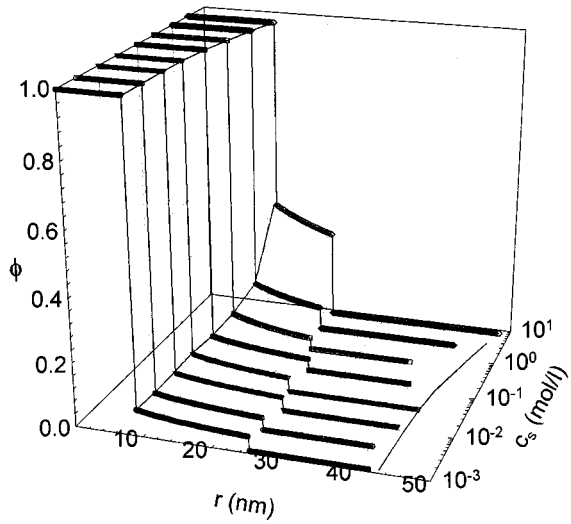

Figure 10. Measured density profiles of the block copolymer micelles for the salt concentrations investigated in the present study.

There is a homogeneous core domain ($0 < r \le R_c$) with a volume fraction $\phi_c = 1$, which is surrounded by the inner part of the micellar corona ($R_c < r \le R_m$). The volume fraction in the inner part is in the range $0.06 < \phi < 0.35$, increasing with increasing salt concentration. The outer part of the corona ($R_m < r \le R_h$) has very low volume fractions $0.007 < \bar{\phi}_{out} < 0.04$. Our attempts to identify the corresponding contribution in the SLS/SANS curves failed, since in the expected q range intermicellar interactions affect the scattering curves considerably. Cryo-TEM images of another polyelectrolyte block copolymer which has much higher electron contrast (poly(butadiene-*b*-*N*-methyl-2-vinylpyridinium iodide)) revealed more structural details of the outer dilute domain, which is the topic of a forthcoming paper.[46] In the case of PEE−PSSH, only the hydrodynamic properties of the micelles are sufficiently affected, so that a measurement of the hydrodynamic radius gives an estimate of the total micellar size. The outer domain seems to have a rather diffuse structure, as it accounts for the considerable fluctuation background at large q. The observed q^{-1} scattering in this regime indicates a stretched conformation of the polyelectrolyte chains.

There have been indications for the presence of a phase separation in the shell of polyelectrolyte block copolymer micelles in previous investigations of PS−PMAc micelles. Electrophoretic mobility measurements on PS−PMAc[47] indicated that a part of the shell experiences a considerable higher ionic stength than the surrounding medium. This had been corroborated by fluorescence studies on PS−PMAc[48−50] and PS−P2VP heteroarm star polymers.[51] According to the steady-state fluorescence and anisotropy decays of fluorophores attached to the ends of the PMAc blocks, a certain fraction of the fluorophores (probably those on the blocks that were folded back to the core/shell interface) monitored a lower polarity of the environment, and their mobility was substantially restricted. Further experimental evidence for the existence of a dense, more hydrophobic inner corona domain has been found in an NMR/SANS study on poly(methyl methacrylate-*b*-acrylic acid) (PMMA−PAAc) micelles.[52]

Interestingly, the corona phase separation has been predicted by Misra et al.[4] and Shusharina et al.[12] for charged brushes in poor solvents. Poor solvent conditions arise from the hydrophobic backbone of the PSSH chain, for which water is a nonsolvent. An indication for poor solvation is the small value of the Flory exponent in the inner corona domain, which is in the range $0.38 \leq \nu \leq 0.44$ as calculated from the value of α (Table 3). For charged brushes in poor solvents, the phase separation should be most pronounced for brushes tethered to convex surfaces because of the strong variation of segment density in the radial direction. It is a consequence of a hierarchy of long-range repulsive forces (electrostatic), medium-range attractive forces (binary attraction of hydrophobic backbone), and short-range repulsive forces (hard-core repulsion of backbone segments) according to de Gennes *n*-cluster theory.

Repulsion between adjacent micelles becomes negligibly small at higher ionic strengths. As a consequence, effects of attractive interactions can become noticeable. The cryo-electron micrograph in Figure 5b was taken from the highest salt concentration at $c_s = 3$ mol/L. The micelles are not homogeneously distributed in the solution but rather form clusters of spatially correlated micelles. The presence of such clusters gives rise to the low-q upturn in the SLS/SANS curves and the low-q downturn in the measured diffusion coefficients. These observations indicate the presence of weak attractive forces that were predicted by Misra et al. concomitant with a corona phase separation under poor solvent conditions.[4,6] Accordingly, short-range attractive forces arise from transient fluctuations in the periphery of the corona, leading at times to attractive interactions between micelles.

4. Conclusions

The structure of polyelectrolyte micelles has been analyzed using a combination of experimental methods including static and dynamic light scattering (SLS, DLS), small-angle neutron scattering (SANS), and cryo-transmission electron microscopy (cryo-TEM). This enabled to determine the internal structure of the micelle as characterized by the micellar core radius, R_c, the micellar radius, R_m, and the hydrodynamic radius, R_h. The micellar core can be well described by a pure homogeneous melt of core-block chains. The micellar corona contains the polyelectrolyte chains that are swollen with solvent and exhibit a segment density that decreases in the radial direction. At low added salt concentrations, the ionic strength of the solution has no influence on the micellar properties, a feature which is typical for an osmotic polyelectrolyte brush. Changes in micellar structure are observed, if the added salt concentration exceeds a value of ca. 0.1 mol/L, which corresponds to the intrinsic ionic strength of the polyelectrolyte shell. Further addition of salt leads to an increase of the corona ionic strength following a simple Donnan-type equilibrium. The concomitant screening of the electrostatic repulsion of the polyelectrolyte chains leads to an increase of the micellar aggregation numbers and micellar core size (salted brush). An unsual feature is the presence of a sharp interface at R_m between an inner and an outer corona domain. This could be independently shown by SANS and cryo-TEM. Beyond R_m there is a significantly smaller segment density of corona chains. This outer corona domain extends probably up to the hydrodynamic radius R_h, as determined by dynamic light scattering. Such a phase-separated corona structure has been predicted for polyelectrolyte brushes under poor solvent conditions by Misra et al.[4] and Shusharina et al.[12]

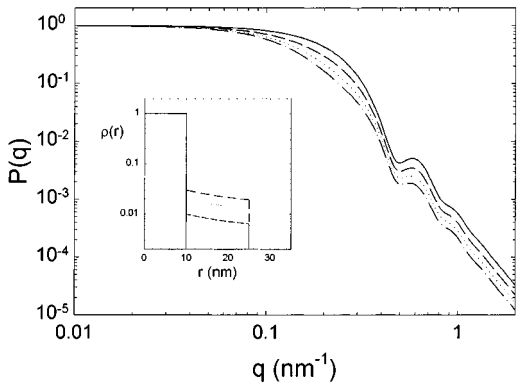

Figure 11. Calculated scattering curves for density profiles common in the present study.

Acknowledgment. We thank I. Below for help with the synthesis of the PS−PB block copolymer. Financial support of the German Science Foundation (Grant Fo246/2-3) and the Dr.-Hermann-Schnell foundation is gratefully acknowledged.

Appendix

The form factor $P(q)$ corresponding to the density profile in eq 11 is given by[53]

$$P_{mic}(q) = \left\{\left[\frac{1}{3}{}_0F_1\left(\frac{3}{2}; -\frac{q^2R_c^2}{4}\right) - \frac{\rho_{int}}{3-\alpha}{}_1F_2\left(\frac{3-\alpha}{2}, \frac{3}{2}, \frac{5-\alpha}{2}; -\frac{q^2R_c^2}{4}\right) + \left(\frac{R_c}{R_m}\right)^{\alpha-3}\frac{\rho_{int}}{3-\alpha}{}_1F_2\left(\frac{3-\alpha}{2}, \frac{3}{2}, \frac{5-\alpha}{2}; \frac{q^2R_m^2}{4}\right)\right]\Big/ \left[\frac{1}{3} - \frac{\rho_{int}}{3-\alpha} + \left(\frac{R_c}{R_m}\right)^{\alpha-3}\frac{\rho_{int}}{3-\alpha}\right]\right\}^2 \quad \text{(A1)}$$

where ${}_0F_1(q,R)$ and ${}_1F_2(q,\alpha,R)$ denote hypergeometric functions. ρ_{int} is given by eq 13. The hypergeometric functions ${}_PF_Q$can be written in terms of series expansions

$${}_0F_1(b_1;x) = \sum_{n=0}^{\infty}\frac{1}{(b_1)_n}\frac{x^n}{n!}$$

$${}_1F_2(a_1,b_1,b_2;x) = \sum_{n=0}^{\infty}\frac{(a_1)_n}{(b_1)_n(b_2)_n}\frac{x^n}{n!} \quad \text{(A2)}$$

where the $(c)_n$ are the Pochhammmer factorials given by

$$(c)_n = \frac{\Gamma(c+n)}{\Gamma(c)} = c(c+1)(c+2)\ldots(c+n-1) \quad \text{(A3)}$$

Many special functions (Hermite's, Bessel's, Laguerre's, Legendre's, etc.) can be written in terms of hypergeometric functions and are thus expressible as a series. This is often the most practical way to obtain numerical values for these functions. The sums in eq A2 can be

easily calculated via the recurrence relation of the Pochhammer factorial $(c)_{n+1} = (c + n)(c)_n$. This enables an efficient implementation of this function in fitting algorithms. Polydispersity of the micelles is taken into account by averaging over a Schulz−Zimm distribution

$$P_x(q) = \int_0^\infty P(q,R)\, h(R)\, \mathrm{d}R$$

$$h(R) = \frac{(z+1)^{z+1}R^z}{\langle R\rangle^{z+1}\Gamma(z+1)} \exp\left[-\frac{(z+1)R}{\langle R\rangle}\right] \qquad \text{(A4)}$$

with the average radius $\langle R\rangle$ and the relative standard deviation $\sigma = (z + 1)^{-1/2}$. The squared expressions $\langle {}_1F_2(...){}_1F_2(...)\rangle$ are given in analytical form in ref 53.

Figure 11 illustrates the contribution of the corona scattering to the form factor of a micelle. Calculated scattering curves for micelles with different corona densities are shown. The density profiles are given in the inset. We notice a characteristic shoulder appearing at $q \approx 0.2$ nm^{-1} with increasing interfacial density.

References and Notes

(1) Förster, S.; Schmidt, M. *Adv. Polym. Sci.* **1995**, *120*, 50.
(2) Barrat, J.-L.; Joanny, J.-F. *Adv. Chem. Phys.* **1996**, *94*, 1.
(3) Miklavic, S. J.; Marcelja, S. *J. Phys. Chem.* **1988**, *92*, 6718.
(4) Misra, S.; Varanasi, S.; Varanasi, P. P. *Macromolecules* **1989**, *22*, 4173.
(5) Zhulina, E. B.; Borisov, O. V.; Birshtein, T. M. *J. Phys. II* **1992**, *2*, 63.
(6) Misra, S.; Mattice, W. L.; Napper, D. H. *Macromolecules* **1994**, *27*, 7090.
(7) Zhulina, E. B. In In *Solvents and Self-Organization of Polymers*; Webber, S. E., Munk, P., Tuzar, Z., Eds.; NATO ASI Series E 327; Kluwer: Dordrecht, The Netherlands, 1996.
(8) Pincus, P. *Macromolecules* **1991**, *24*, 2912.
(9) Argillier, J. F.; Tirrell, M. *Theor. Chim. Acta* **1992**, *82*, 343.
(10) Marko, J. F.; Rabin, Y. *Macromolecules* **1992**, *25*, 1503.
(11) Dan, N.; Tirrell, M. *Macromolecules* **1993**, *26*, 4310.
(12) Shusharina, N. P.; Nyrkova, I. A.; Khokhlov, A. R. *Macromolecules* **1996**, *29*, 3167.
(13) Selb, J.; Gallot, Y. In *Developments in Block Copolymers*, 2nd ed.; Goodman, I., Ed.; Elsevier: Amsterdam, 1985.
(14) Selb, J.; Gallot, Y. *Makromol. Chem.* **1980**, *181*, 809.
(15) Tuzar, Z. In *Solvents and Self-Organization of Polymers*; Webber, S. E., Munk, P., Tuzar, Z., Eds.; NATO ASI Series E 327; Kluwer: Dordrecht, The Netherlands, 1996.
(16) Zhang, L. F.; Eisenberg, A. *Science* **1995**, *268*, 1728.
(17) Zhang, L. F.; Barlow, R. J.; Eisenberg, A. *Macromolecules* **1995**, *28*, 6055.
(18) Khougaz, K.; Astafieva, I.; Zhong, X. F.; Eisenberg, A. *Macromolecules* **1995**, *28*, 7135.
(19) Gao, Z.; Varshney, S. K.; Wong, S.; Eisenberg, A. *Macromolecules* **1994**, *27*, 7923.
(20) Moffitt, M.; Khougaz, K.; Eisenberg, A. *Acc. Chem. Res.* **1996**, *29*, 95.
(21) Valint, L.; Bock, J. *Macromolecules* **1988**, *21*, 175.
(22) Astafieva, I.; Zhong, X. F.; Eisenberg, A. *Macromolecules* **1993**, *26*, 7339.
(23) Astafieva, I.; Khougaz, K.; Zhong, X. F.; Eisenberg, A. *Macromolecules* **1995**, *28*, 7127.
(24) Guenoun, P.; Davis, H. T.; Tirrell, M.; Mays, J. W. *Macromolecules* **1996**, *29*, 3965.
(25) Guenoun, P.; Lipsky, S.; Mays, J. W.; Tirrell, M. *Langmuir* **1996**, *12*, 1425.
(26) Guenoun, P.; Muller, F.; Delsanti, M.; Auvray, L.; Chen, Y. J.; Mays, J. W.; Tirrell, M. *Phys. Rev. Lett.* **1998**, *81*, 3872.
(27) Guenoun, P.; Schlachli, A.; Sentenac, D.; Mays, J. W.; Benattar, J. J. *Phys. Rev. Lett.* **1995**, *74*, 3628.
(28) Hariharan, R.; Biver, C.; Mays, J. W.; Russell, W. B. *Macromolecules* **1998**, *31*, 7506.
(29) Hariharan, R.; Biver, C.; Russell, W. B. *Macromolecules* **1998**, *31*, 7514.
(30) Tauer, K.; Müller, H.; Rosengarten, L.; Riedelsberger, K. *Colloids Surf. A* **1999**, *153*, 75.
(31) Ahrens, H.; Förster, S.; Helm, C. A. *Macromolecules* **1998**, *30*, 88447.
(32) Ahrens, H.; Förster, S.; Helm, C. A. *Phys. Rev. Lett.* **1998**, *81*, 4172.
(33) Förster, S.; Hermsdorf, N.; Leube, W.; Schnablegger, H.; Regenbrecht, M.; Akari, S.; Lindner, P.; Böttcher, C. *J. Phys. Chem. B* **1999**, *103*, 6652.
(34) Lindner, P. In *Modern Aspects of Small-Angle Scattering*; Brumberger, H., Ed.; NATO Advanced Study Institutes, Ser. C, Vol. 451; Kluwer Academic: London, 1993.
(35) Böttcher, C.; Stark, H.; van Heel, M. *Ultramicroscopy* **1996**, *62*, 133.
(36) Neugebauer, T. *Ann. Phys.* **1943**, *42*, 509.
(37) Ashcroft, N. W.; Lekner, J. *Phys. Rev.* **1966**, *45*, 33.
(38) Förster, S.; Schmidt, M. *Adv. Polym. Sci.* **1995**, *120*, 51.
(39) Förster, S.; Schmidt, M.; Antonietti, M. *Polymer* **1990**, *31*, 781.
(40) Daoud, M.; Cotton, J. P. *J. Phys. (Paris)* **1982**, *43*, 531.
(41) Förster, S.; Wenz, E.; Lindner, P. *Phys. Rev. Lett.* **1996**, *77*, 95.
(42) Willner, L.; Poppe, A.; Allgaier, J.; Monkenbusch, M.; Lindner, P.; Richter, D. *Europhys. Lett.* **2000**, *51*, 628.
(43) Teixera, J. *J. Appl. Crystallogr.* **1988**, *21*, 781.
(44) Förster, S.; Zisenis, M.; Wenz, E.; Antonietti, M. *J. Chem. Phys.* **1996**, *104*, 9956.
(45) Antonietti, M.; Bremser, W.; Schmidt, M. *Macromolecules* **1990**, *23*, 3796.
(46) Förster, S.; Plantenberg, T.; Hermsdorf, N.; Böttcher, C.; Lindner, P., manuscript in preparation.
(47) Tuzar, Z.; Prochazka, K.; Zuskova, I.; Munk, P. *Polym. Prepr.* **1993**, *31*, 1038.
(48) Prochazka, K.; Kiserow, D.; Ramireddy, C.; Webber, S. E.; Munk, P.; Tuzar, Z. *Makromol. Chem., Macromol. Symp.* **1992**, *58*, 201.
(49) Stepanek, M.; Podhajecka, K.; Prochazka, K.; Teng, Y.; Webber, S. E. *Langmuir* **1999**, *15*, 4185.
(50) Stepanek, M.; Prochazka, K.; Brown, W. *Langmuir* **2000**, *16*, 2502.
(51) Tsitsilianis, C.; Voulgaris, D.; Stepanek, M.; Podhajecka, K.; Prochazka, K.; Tuzar, Z.; Brown, W. *Langmuir* **2000**, *16*, 6868.
(52) Kriz, J.; Basar, B.; Pospisil, H.; Plestil, J.; Tuzar, Z.; Kiselev, M. A. *Macromolecules* **1996**, *29*, 7853.
(53) Förster, S.; Burger, C. *Macromolecules* **1998**, *31*, 879.

MA011565Y